SAGE-Hindawi Access to Research
Biotechnology Research International
Volume 2011, Article ID 854068, 15 pages
doi:10.4061/2011/854068

Research Article

Human Coronary Artery Smooth Muscle Cell Responses to Bioactive Polyelectrolyte Multilayer Interfaces

Robert G. Newcomer,[1] Maroun D. Moussallem,[1] Thomas C. S. Keller,[2] Joseph B. Schlenoff,[1] and Qing-Xiang Amy Sang[1]

[1] *Department of Chemistry and Biochemistry, Institute of Molecular Biophysics, The Florida State University, 3501 Chemical Sciences Laboratory Building, 102 Varsity Way, Tallahassee, FL 32306-4390, USA*
[2] *Department of Biological Science, The Florida State University, Tallahassee, FL 32306, USA*

Correspondence should be addressed to Qing-Xiang Amy Sang, sang@chem.fsu.edu

Received 10 August 2010; Accepted 5 October 2010

Academic Editor: Goetz Laible

Under normal physiological conditions, mature human coronary artery smooth muscle cells (hCASMCs) exhibit a "contractile" phenotype marked by low rates of proliferation and protein synthesis, but these cells possess the remarkable ability to dedifferentiate into a "synthetic" phenotype when stimulated by conditions of pathologic stress. A variety of polyelectrolyte multilayer (PEMU) films are shown here to exhibit bioactive properties that induce distinct responses from cultured hCASMCs. Surfaces terminated with Nafion or poly(styrenesulfonic acid) (PSS) induce changes in the expression and organization of intracellular proteins, while a hydrophilic, zwitterionic copolymer of acrylic acid and 3-[2-(acrylamido)-ethyl dimethylammonio] propane sulfonate (PAA-*co*-PAEDAPS) is resistant to cell attachment and suppresses the formation of key cytoskeletal components. Differential expression of heat shock protein 90 and actin is observed, in terms of both their magnitude and cellular localization, and distinct cytoplasmic patterns of vimentin are seen. The ionophore A23187 induces contraction in confluent hCASMC cultures on Nafion-terminated surfaces. These results demonstrate that PEMU coatings exert direct effects on the cytoskeletal organization of attaching hCASMCs, impeding growth in some cases, inducing changes consistent with phenotypic modulation in others, and suggesting potential utility for PEMU surfaces as a coating for coronary artery stents and other implantable medical devices.

1. Introduction

Vascular smooth muscle cells (VSMCs) are implicated as key contributors to numerous vascular pathologies, including atherosclerosis and the restenosis of angioplasty-treated blood vessels in the presence or absence of coronary stents, given their remarkable capacity for phenotypic modulation in response to pathological stressors [1–7]. Rather than achieving a state of terminal differentiation upon maturity, VSMCs are capable of dedifferentiation through apparently reversible pathways, as they transition between a "contractile" state marked by low rates of proliferation and protein synthesis, and a "synthetic" state marked by an increase in these parameters. An unknown number of transitional states likely reside between these two extremes, and the possibility that the transitory pathways between these two phenotypic states may not be identical lends additional complexity to this scenario [7]. There is also evidence that phenotypically heterogeneous subpopulations of VSMCs may exist within the arterial media itself [2, 6], but when placed into *in vitro* culture systems, all SMCs tend to exhibit a synthetic phenotype [6].

Phenotypic modulation of VSMCs has been reported *in vitro* utilizing serum deprivation and readministration [8], or growth surfaces coated with type IV collagen at specific passages and time points of primary VSMC cultures [3]. For this study, the potential utility of thin polyelectrolyte multilayer (PEMU) films in the induction of phenotypic modulation in such cells is explored. The PEMUs incorporated into this study were generated utilizing layer-by-layer deposition [9, 10], in which a substrate is moved back and forth between dilute baths of positively and negatively

charged polyelectrolyte solutions, and multiple iterations of this process allow for the gradual, controlled buildup of these coatings. The surfaces generated are uniform, durable, and reproducible, and this process also allows for the coating of substrates with complex geometries, such as the mesh-tube geometry of implantable stenting devices.

PEMUs have been used to successfully control the attachment of a variety of cell types including fibroblasts [11], primary hepatocytes [12], and neuron-like cells [13] and have also been used to promote the colonization and direct the differentiation of endothelial progenitor cells for vascular grafts [14–18]. Previous studies utilizing a rat aortic smooth muscle cell line (A7r5) cultured on different PEMUs have revealed changes suggestive of phenotypic modulation [19–21], including variations in the mRNA expression of smooth muscle α-actin, vimentin, and transgelin, an early marker of SMC differentiation [21, 22].

The potential biological applications of cell culture substrates are likely dependent on the ability of these surfaces to mimic biological microenvironments [23]. The aim of this study was to determine if SMCs derived from the human coronary artery (hCASMCs) and cultured on different PEMU surfaces exhibited detectable variations suggestive of phenotypic modulation, corresponding to different physiological microenvironments that can occur in response to arterial injury, such as may occur during stent implantation. Observable changes that were considered included morphology, growth, contractility, and protein expression in terms of both its magnitude and intracellular localization.

2. Materials and Methods

2.1. Reagents. 1,3-Propane sulfone (PS), acrylic acid (AA), poly(styrenesulfonic acid) (PSS; MW 7.3×10^4), poly(diallyldimethylammonium chloride) (PDADMAC; MW 3.7×10^5), poly(allylamine hydrochloride) (PAH; MW $\approx 7 \times 10^4$), and poly(acrylic acid) (PAA; MW $\approx 2.4 \times 10^5$) were used as received from Aldrich. 2-(Acrylamido)-ethyl dimethylamine (AEDA) was obtained from Monomer-Polymer & Dajac Inc. Poly(4-vinyl pyridine) (P4VP; MW $\approx 5 \times 10^4$) was obtained from Polymer Source, Inc. Nafion, a perfluorinated sulfonated polymer, was purchased from Aldrich and used as a 0.3 wt% solution in ethanol : methanol 50 : 50 (vol/vol). All polymers (except fluorinated polymers), monomer, and buffer solutions were prepared using 18 MΩ water. Commercial antibodies were obtained from Santa Cruz [HSP90 (H-114), isoforms of actin (I-19)] and Sigma-Aldrich [α-smooth muscle actin (1A4), vimentin (V9)]. Normal mouse IgG controls were obtained from Biomeda, and normal rabbit IgG controls were purified from rabbit serum by our laboratory. Alkaline phosphatase- (AP-) conjugated secondary antibodies were obtained from Sigma-Aldrich and fluorophore-conjugated secondary antibodies (Alexa Fluor 488 and 546) were purchased from Molecular Probes (Invitrogen). Unless noted otherwise, all components of routine buffering systems were obtained from Sigma-Aldrich.

2.2. Polyelectrolyte Synthesis. The PAA-*co*-PAEDAPS copolymer was prepared from 3-[2-(acrylamido)-ethyl dimethylammonio] propane sulfonate (AEDAPS) [19] and AA via free radical polymerization as described by McCormick and Salazar [24], with a 90 : 10 AA : AEDAPS molar ratio. The polymers were characterized using Fourier transform infrared (FTIR) and attenuated total reflection FTIR, which confirmed the presence of carbonyl bond stretch C=O ($1725\,cm^{-1}$, AA; $1670\,cm^{-1}$, AEDAPS) and sulfonate bond (νSO_3^-) stretch at $\sim 1200\,cm^{-1}$. Poly(4-vinyl-trideca-fluoro-octyl pyridinium iodide)-co-poly(4-vinyl pyridine) (PFPVP) was synthesized to obtain a positively charged perfluorinated polyelectrolyte for layering with the negatively charged Nafion [25], and this polymer exhibited the distinctive C-F bond stretch in the 1200-cm^{-1} region of the IR spectrum.

2.3. PEMU Coating on Glass Coverslips. Glass coverslips (Corning no. 1.5, 22 mm^2) were first cleaned in 70% H_2SO_4 (concentrated)/30% $H_2O_{2(aq)}$ ("piranha", a strong oxidizer that should not be stored in a closed container). The cleaned coverslips were rinsed in water and blown dry with a stream of nitrogen. Polymer solution concentrations were at 10 mM (with respect to the monomer repeat unit) in a 0.15 M sodium chloride salt solution, with the exception of Nafion, which was prepared as a 0.3 wt% solution in ethanol:methanol 50 : 50 vol/vol. Sequential adsorption of polyelectrolytes onto the coverslips was performed by automated deposition for 10 min in each polymer solution followed by three rinses with water for 1 min each.

2.4. PEMU Nomenclature. For clarity, the following shorthand is adopted for multilayers: $(A/B)_x$ where A is the starting polyelectrolyte contacting the substrate (coverslip), B is the terminating polyelectrolyte layer contacting the cells, and x is the number of layer pairs.

2.5. Culture of hCASMCs. Human coronary artery smooth muscle cells (hCASMCs) (BioWhittaker, Inc.) were routinely cultured in Smooth Muscle Basal Medium (SmBM, Cambrex) in which 475 mL of SmBM was supplemented with 0.5 mL human epidermal growth factor (hEGF), 0.5 mL insulin, 1.0 mL human fibroblast growth factor B (hFGF-B) (all from Cambrex at 1 μg/mL, SmGM-2 SingleQuots), 25 mL (5%) fetal bovine serum (FBS) (Cambrex), and 0.5 mL gentamicin/amphotericin-B (GA-1000) (Cambrex). Cells were maintained at 37°C in a humidified atmosphere containing 5% CO_2. All PEMU-coated coverslips were equilibrated by contact with warm SmBM prior to cell seeding. All cell-based assays utilized cell passages of 6 or less.

2.6. Growth Assays. Cell suspensions in SmBM were seeded onto coated or uncoated glass coverslips (Corning no. 1.5) at a uniform density of 10,000 cells/cm^2 and housed in 6-well polystyrene tissue culture plates (Becton Dickinson) for a period of five days with fresh media added on the second and fourth days. Coverslips were gently dipped in phosphate-buffered saline (PBS) prior to trypsinization of all attached cells, and the total number of cells recovered from

each coverslip was determined by hemocytometer. Assays were repeated three times, and variations between the mean values were analyzed using the least significant difference correction for one-way analysis of variance (ANOVA) for multiple comparisons (Analyse-It for Microsoft Excel). Data represent the mean ± S.E. from three separate experiments.

2.7. Two-Dimensional Gel Electrophoresis. Cultured hCASMCs grown on coated or uncoated glass coverslips as described were rinsed gently with PBS then lysed with minimal buffer containing 7 M urea, 2 M thiourea, 2% 3-[(3-cholamidopropyl)dimethylammonio]-1-propanesulfonate (CHAPS), 65 mM dithiothreitol (DTT) and a broad-spectrum protease inhibitor cocktail (Sigma, P2714). Cells were removed with a cell scraper and transferred to a siliconized tube for centrifugation at 17,000 × g for 20 min at 4°C. The supernatant was recovered and the precipitate was discarded. The protein content of the collected fractions was determined using the Coomassie Plus-Better Bradford Assay Kit (Pierce), bovine serum albumin (BSA) standards, and four replicates of each sample. Isoelectric focusing (IEF), the first dimension of separation, was accomplished utilizing a Protean IEF Cell apparatus (Bio-Rad). Protein samples were diluted into lysis buffer supplemented with ampholytes (Bio-Rad) and fresh DTT prior to active rehydration at 50 V for 12 h at 20°C using 11 cm ReadyStrip Immobilized pH Gradient (IPG) strips, pH 4 to 7 (Bio-Rad). Following rehydration, the proteins were focused at 250 V for 15 min, and then 8000 V was maintained for a total of 60,000 Vh/gel. For the second dimension of separation, the IPG strips were first equilibrated for 10 min in 2.5 mL of a solution consisting of 375 mM Tris-HCl (pH 8.8), 6 M urea, 2% SDS, and 2% DTT, followed by a second equilibration, for an additional 10 min, in 2.5 mL of a second equilibration buffer composed of 375 mM Tris-HCl (pH 8.8), 6 M urea, 2% SDS, and 2.5% iodoacetamide. The equilibrated IPG strips were washed with cathode buffer (0.1 M Tricine, 0.1 M Tris-HCl (pH 8.2), and 0.1% SDS) prior to separation on a 10% polyacrylamide gel hand-casted using Criterion Cassettes (Bio-Rad). The anode buffer was a 2 M Tris-HCl (pH 8.9) solution. Gels were electrophoresed at 50 V for 30 min, then at 100 V until the end of the separation. Gels were fixed in 50% methanol/7% acetic acid prior to staining with SYPRO Ruby (Bio-Rad) and imaging with Typhoon Scanning Systems (GE Healthcare). Gels were processed and compared using ImageMaster 2D Platinum v6.0 (Amersham).

2.8. Matrix-Assisted Laser Desorption Ionization: Time of Flight Mass Spectrometry (MALDI-TOF MS). Spots of interest were excised for in-gel tryptic digestion. Excised fragments were placed into a siliconized tube and exposed to acetonitrile (ACN) for 15 min. The shrunken fragments were then allowed to air-dry prior to digestion with activated trypsin (Pierce) at approximately 100 ng/sample in a buffer containing 25 mM ammonium bicarbonate. Proteins contained within the gel fragments were digested at 30°C overnight with agitation at 1500 rpm. All tubes were briefly centrifuged the next morning, and the supernatant was separated from the gel plug. All samples extracted from the gel plugs were desalted with ZipTip C18 Tips (Millipore) and eluted with a matrix solution comprised of α-cyano-4-hydroxycinnamic acid (CHCA) (Sigma) at 4 mg/mL dissolved in 50% ACN/0.1% triflouroacetic acid (TFA) (Sigma). Eluted samples were applied directly to a MALDI-TOF MS target plate and allowed to dry prior to analysis utilizing an Axima CFR+ MALDI-TOF Mass Spectrometer (Shimadzu Biotech). Spectra were calibrated to known standards using the ProteoMass Peptide MALDI-MS Calibration Kit (Sigma) incorporating five standard peptides. All spectra were composed of 175 profiles for each sample, and were processed using Kompact Software (Kratos Analytical). Proteins were identified by their peptide mass fingerprint (PMF) utilizing MASCOT software against the NCBI and Swiss-Prot databases, specifying monoisotopic peaks of human taxonomy, 1 missed cleavage, and a peptide tolerance of ±1 Da. Fixed and variable chemical modifications, including the carbamidomethylation of cysteine and the oxidation of methionine, respectively, were taken into consideration for these queries. Identities were accepted or rejected based upon the extent of sequence coverage, the magnitude of the MOlecular Weight SEarch (MOWSE) probability score (>54), and the accuracy of both the pI and molecular mass of the candidate protein.

2.9. Western Blotting. Aliquots of cell lysates in the previously described buffer containing equal volumes (5 μg) of total protein were combined with an SDS-containing buffer (50 mM Tris, pH 6.7, 20 mM ethylenediaminetetraacetic acid (EDTA), 5% Sucrose, 1.5% SDS, trace bromophenol blue, and 1% fresh β-mercaptoethanol) prior to separation by electrophoresis on 8% polyacrylamide gels. The proteins contained in the gels were then transferred to a nitrocellulose membrane utilizing 3-(cyclohexylamino)-1-propane sulfonic acid (CAPS) buffer (100 mM, pH 11) and a current of 50 volts for 90 min at ambient temperature. Blots were blocked overnight at 4°C with gentle agitation in Tris-buffered saline (TBS, pH 7.5) containing 4% BSA. Primary antibodies and AP-conjugated secondary antibodies were used at manufacturer-recommended dilutions, with incubation periods of two hours at ambient temperatures. Positive bands were visualized following the addition of 5-bromo-4-chloro-3-indoyl phosphate and nitro blue tetrazolium (both from Fisher Scientific). Blotted membranes were scanned and analyzed by integrated morphometry analysis (Metamorph Systems) utilizing a uniform threshold for each blotted membrane. Variations between the mean values were analyzed using the least significant difference correction for one-way ANOVA for multiple comparisons. Data represent the mean ± S.E. from three separate experiments.

2.10. Immunofluorescence Confocal Microscopy. Cells grown on each surface were washed twice with warm PBS (37°C) prior to fixation with ice-cold methanol (−20°C) for five min (for actin and vimentin) or warm 3.7% paraformaldehyde in 50% PBS and 50% SmBM for 15 min (for HSP90). Following another PBS wash, cells to be stained for HSP90 were

permeabilized with 0.2% Triton X-100 in PBS for 15 min. All cells were washed three times with 0.05% Triton X-100 in PBS (PBST), and were treated identically from this point forward. Samples were blocked with Image-iT FX Signal Enhancer (Invitrogen) for 30 min at room temperature in a humid environment prior to incubation with primary antibodies diluted in PBST for 60 min, and purified preimmune IgGs from the same species were utilized as negative controls. Following another washing phase, samples were incubated for 60 min in a dark environment with Alexa Fluor 488 or Alexa Fluor 546 (Invitrogen) secondary detection conjugates diluted 1 : 250 in PBST. After a final washing phase, samples were dried and mounted using ProLong Gold antifade reagent with 4′,6-diamidino-2-phenylindole (DAPI) (Invitrogen), and were allowed to cure in a dark environment for no less than 18 hours prior to visualization of fluorescent signals with a Zeiss LSM510 laser scanning confocal microscope (Carl Zeiss, Germany) equipped with a multiphoton laser. Wide-field images of fluorescent signals were acquired using a Nikon Microphot FX equipped with a 100X objective and a Zeiss Axiocam.

2.11. Contraction Assays. Cells were cultured as previously described. After five days growth, the calcium ionophore A23187 (free acid, 98%, Fisher Scientific) was introduced into wells at a final concentration of 1 μM. Stock concentrations of 50 mM were first prepared in anhydrous dimethyl sulfoxide (DMSO, Fisher Scientific), which was then diluted into warm SmBM prior to addition. Equivalent volumes of SmBM/DMSO alone were utilized for control experiments. Contraction was monitored using a Zeiss Axiovert 35 microscope in conjunction with a Hamamatsu Digital Camera and Uniblitz Shutter Driver. Time-lapse image stacks were processed using Metamorph Systems (Universal Imaging Corp.).

3. Results

3.1. Cell Morphology and Growth on PEMU Surfaces. A thickness of two-layer pairs is sufficient to coat the surface of a glass substrate with few dispersed bumps [19, 26], and given the thinness of these coatings the underlying glass provided the dominant contribution to stiffness [27], which allowed the effects of chemical modifications at the cell-substrate interface to be explored. Cells on uncoated glass (Figure 1(a)) and $(PFPVP/Nafion)_2$ (Figure 1(b)) displayed a typical stellate morphology, and were indistinguishable from one another during the early phases of a new culture. Cells on $(PDADMA/PSS)_2$ (Figure 1(c)) showed a marked tendency towards aggregation, and with a higher percentage of cells exhibiting membrane ruffling. Very few cells attached to the $(PAH/PAA\text{-}co\text{-}PAEDAPS)_2$ surface, and those that did were almost exclusively rounded as opposed to flat, with numerous filopodia-like extensions of the cell membrane extending in all directions (Figure 1(d)). The $(PAH/PAA\text{-}co\text{-}PAEDAPS)_2$ cultures never exhibited appreciable signs of proliferation after this initial period of attachment (Figure 1(h)), even when cultures were maintained for periods in excess of two weeks (data not shown). After five days of growth, the number of cells obtained from the $(PFPVP/Nafion)_2$ and $(PDADMA/PSS)_2$ surfaces were statistically identical, and approximately half that obtained from glass surfaces (Table 1). While the cells coated on glass formed a uniform, confluent layer, covering the entire surface of the coverslips (Figure 1(e)), the cultures on the $(PFPVP/Nafion)_2$ surfaces exhibited a "hill and valley" morphology [5, 28], in which dense clusters of cells were interspersed with areas that were more sparsely populated (Figure 1(f)). The cells on $(PDADMA/PSS)_2$ exhibited a lasting tendency for aggregation, with an appearance most similar to that of the $(PFPVP/Nafion)_2$ cultures (Figure 1(g)). For both the $(PFPVP/Nafion)_2$ and $(PDADMA/PSS)_2$ cultures, the cells did not spread to the outer edges of the coverslip (data not shown), which accounts for a significant fraction of their diminished numbers.

Table 1: Cell growth after 5 days on PEMU surfaces.

Growth surface	Cells/cm^2	SE	% Decrease from glass	CI = 99%
Uncoated Glass	19782	±1500	—	**
$(PFPVP/Nafion)_2$	9038	±400	54.3%	*
$(PDADMA/PSS)_2$	8918	±1300	54.9%	*
$(PAH/PAA\text{-}co\text{-}PAEDAPS)_2$	619	±200	96.9%	**

*significant variation from glass and $(PAH/PAA\text{-}co\text{-}PAEDAPS)_2$ only; **significant variation from all groups; data are reported as the mean ± standard error (SE) of three separate experiments; CI: confidence interval.

3.2. Differential Protein Expression on PEMU Surfaces. The possibility of differential protein expression in these culture systems was investigated by two-dimensional gel electrophoresis (2DE), although the cell-resistant $(PAH/PAA\text{-}co\text{-}PAEDAPS)_2$ surface did not yield enough cells for inclusion into this phase of analysis. Six parallel cultures were pooled, and similar patterns of expression were revealed (Figure 2). A comparison between the glass and $(PDADMA/PSS)_2$ sample gels yielded a total of 390 protein spots on the "Master gel" (a composite of both gel sets), where variations in the "% volume" of the spots (normalizing the spot volumes of the individual gels) in excess of 50% were observed in 117 spots. Using identical methods and criteria, a comparison between the glass and $(PFPVP/Nafion)_2$ gels also yielded 390 spots, with variations in 229 spots, while a direct comparison between $(PDADMA/PSS)_2$ and $(PFPVP/Nafion)_2$ yielded 339 spots, with variations indicated in 147 spots. Of the candidate proteins excised from these gels and identified (Figure 3), differential expression was further supported by Western blot analyses in two instances (Figure 4). The highest levels of heat shock protein 90 (HSP90) expression were consistently observed in hCASMCs collected from $(PDADMA/PSS)_2$ growth surfaces (Figure 4(a)), and its expression was 8.4% higher than that seen on glass (CI = 95%), while the highest expression of actin was consistently observed in hCASMCs collected from $(PFPVP/Nafion)_2$ (Figure 4(b)), and was 38.6% higher than that seen on

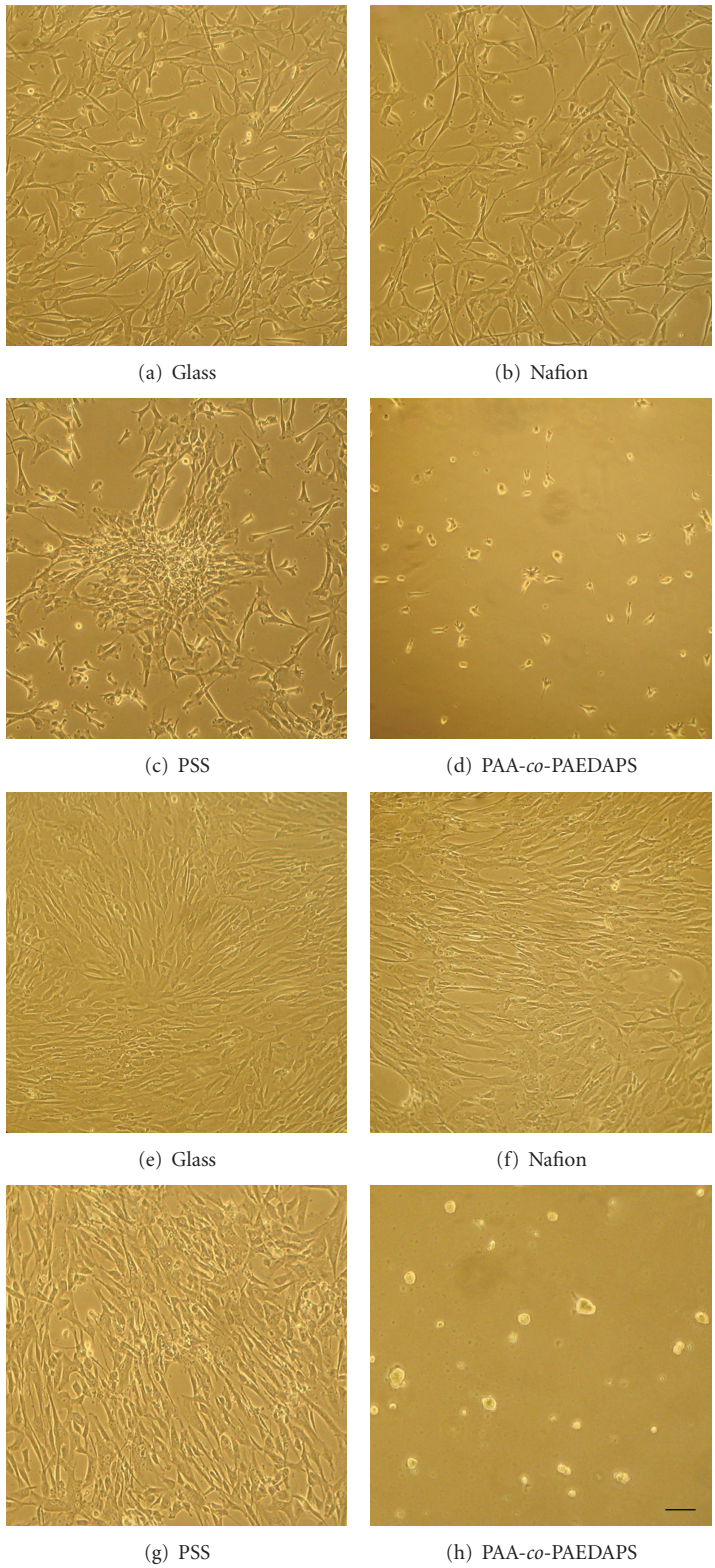

(a) Glass (b) Nafion

(c) PSS (d) PAA-*co*-PAEDAPS

(e) Glass (f) Nafion

(g) PSS (h) PAA-*co*-PAEDAPS

Figure 1: Morphology of hCASMC cultures on PEMU surfaces after 24 hours on (a) uncoated glass, (b) $(PFPVP/Nafion)_2$, (c) $(PDADMA/PSS)_2$, and (d) $(PAH/PAA\text{-}co\text{-}PAEDAPS)_2$. After 5 days, hCASMCs on (e) uncoated glass achieved a uniform, confluent layer, while cells on (f) $(PFPVP/Nafion)_2$ exhibited a "hill and valley" morphology. Cells on (g) $(PDADMA/PSS)_2$ exhibited continued aggregation with a pattern similar to that seen on $(PFPVP/Nafion)_2$, but with less alignment of the cells. Cultures on (h) $(PAH/PAA\text{-}co\text{-}PAEDAPS)_2$ were virtually unchanged after 5 days. All images are 100x. Scale bar = 20 μm.

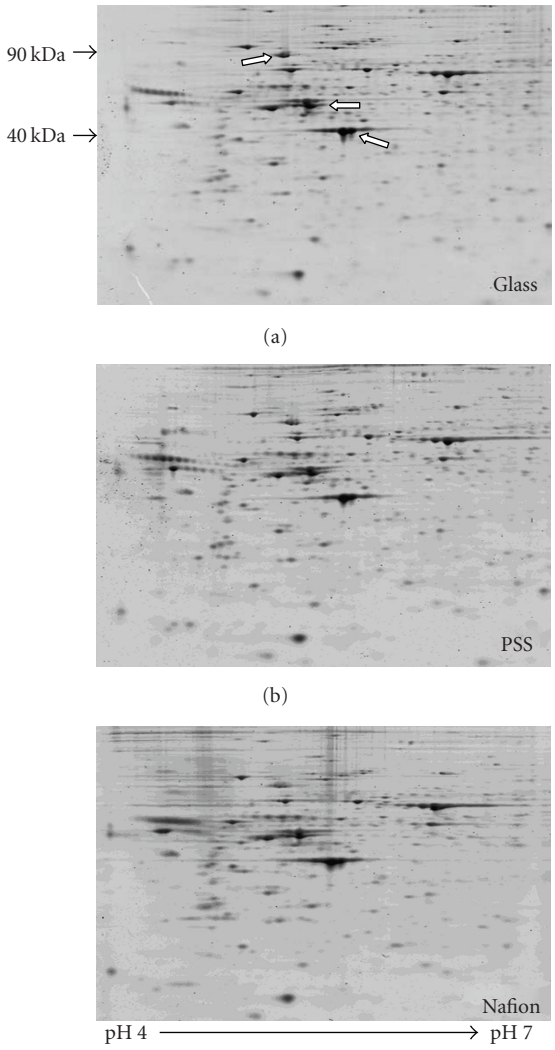

Figure 2: Two-dimensional separation of hCASMC lysates harvested from uncoated glass (top), $(PDADMA/PSS)_2$ (bottom left), and $(PFPVP/Nafion)_2$ (bottom right). Representative gels show the separation of 50 μg of total protein separated from pH 4 to 7 on a 10% polyacrylamide gel stained with SYPRO Ruby and imaged with Typhoon Scanning Systems. White arrows correspond to excised spots that were identified as HSP90 (top-left; MW: 85 kDa, pI: 4.9, with α and β isoforms sharing these approximate values), actin (bottom-right; MW 42 kDa, pI: 5.2, with the β, γ, and α-SM isoforms sharing these approximate values), and vimentin (center; MW: 53 kDa, pI: 5.1).

$(PDADMA/PSS)_2$ (CI = 90%). Differences in the mean abundance of vimentin were not significant by Western blotting (data not shown).

For HSP90, Mascot search algorithms returned a significant MOWSE (MOlecular Weight SEarch) probability score for both the β (MOWSE: 123) and α (MOWSE: 71) isoforms of this protein (Figure 3(a)), with sequence coverages of 40% and 34%, respectively. The two isoforms of human HSP90, designated α and β, are more than 85% identical, and there is only limited evidence in mammalian cells for functional differences between the two [29]. Given the relative similarities between the α and β isoforms of HSP90 in terms of their molecular mass (α: 85 kDa, β: 83.5 kDa) and pI (α: 4.94, β: 4.97), with significant MOWSE scores obtained for either isoform, it was therefore considered that the entirety of the excised spot was most likely some combination of both isoforms. For actin, identical MOWSE scores of 103 were returned for both the β and γ isoforms (Figure 3(b)), with a similarly identical sequence coverage for both forms, at 51%. Of the multiple isoforms of actin that have been identified in mammalian smooth muscle, β actin is the most widely expressed, while the α-SM actin isoform is highly expressed in vascular smooth muscle, and is specialized for contractile structures [3, 30]. The different isoforms of actin exhibit 95% homology in their amino acid sequence [30], and as with the HSP family of proteins, given the relative similarities between the actin isoforms in terms of their molecular weight (α-SM: 42.3 kDa, β: 42.1 kDa, γ: 42.1 kDa) and pI (α-SM: 5.23, β: 5.29, γ: 5.31), it is again considered that the entirety of the excised spot was composed of some combination of actin isoforms.

3.3. Intracellular Localization of HSP90. Given the relatively small magnitude of variation in HSP90 expression, fluorescent immunological cell staining was undertaken to study the possible cellular context of this difference. HSP90 has previously been found preferentially localized in the ruffling membranes of adherent mouse lymphoma cells [31], and hCASMCs cultured on $(PDADMA/PSS)_2$ display a similar localization, designated by yellow arrows (Figure 5(c)), that is absent on glass (Figure 5(a)), $(PFPVP/Nafion)_2$ (Figure 5(b)), or $(PAH/PAA\text{-}co\text{-}PAEDAPS)_2$ (Figure 5(d)).

3.4. Intracellular Localization of Actin Isoforms. Fluorescent studies of actin also support a pattern of differential protein expression on PEMU surfaces, particularly in terms of the α-smooth muscle actin (α-SM actin) isoform (Figure 6). Immunocytochemical double staining for multiple actin isoforms (Figures 6(a), 6(c), 6(e), and 6(g)), with α-SM actin in green, the remaining isoforms in red, and blue nuclear staining with DAPI, suggests that differential actin expression arises primarily from changes in the α-SM actin isoform. On glass (Figure 6(a)), $(PDADMA/PSS)_2$ (Figure 6(c)), and $(PFPVP/Nafion)_2$ (Figure 6(e)), expression of the non-α isoforms (in red) appears fairly uniform, particularly when compared to the expression of α-SM actin (in green) on the $(PFPVP/Nafion)_2$ surface, where intense staining of α-SM actin filaments can be seen throughout the entirety of the cell. Of particular note on the glass and $(PDADMA/PSS)_2$ surfaces is the relative absence of actin filaments in the perinuclear regions, which may be associated with the increased presence of organelles in these areas associated with protein synthesis and a synthetic phenotype [3]. On the $(PAH/PAA\text{-}co\text{-}PAEDAPS)_2$ surface (Figure 6(g)), the isoforms of actin are seen primarily at the cell perimeter, and even after five days, multiple thin filopodia extend from the cell in every direction seeking purchase on this in-hospitable surface.

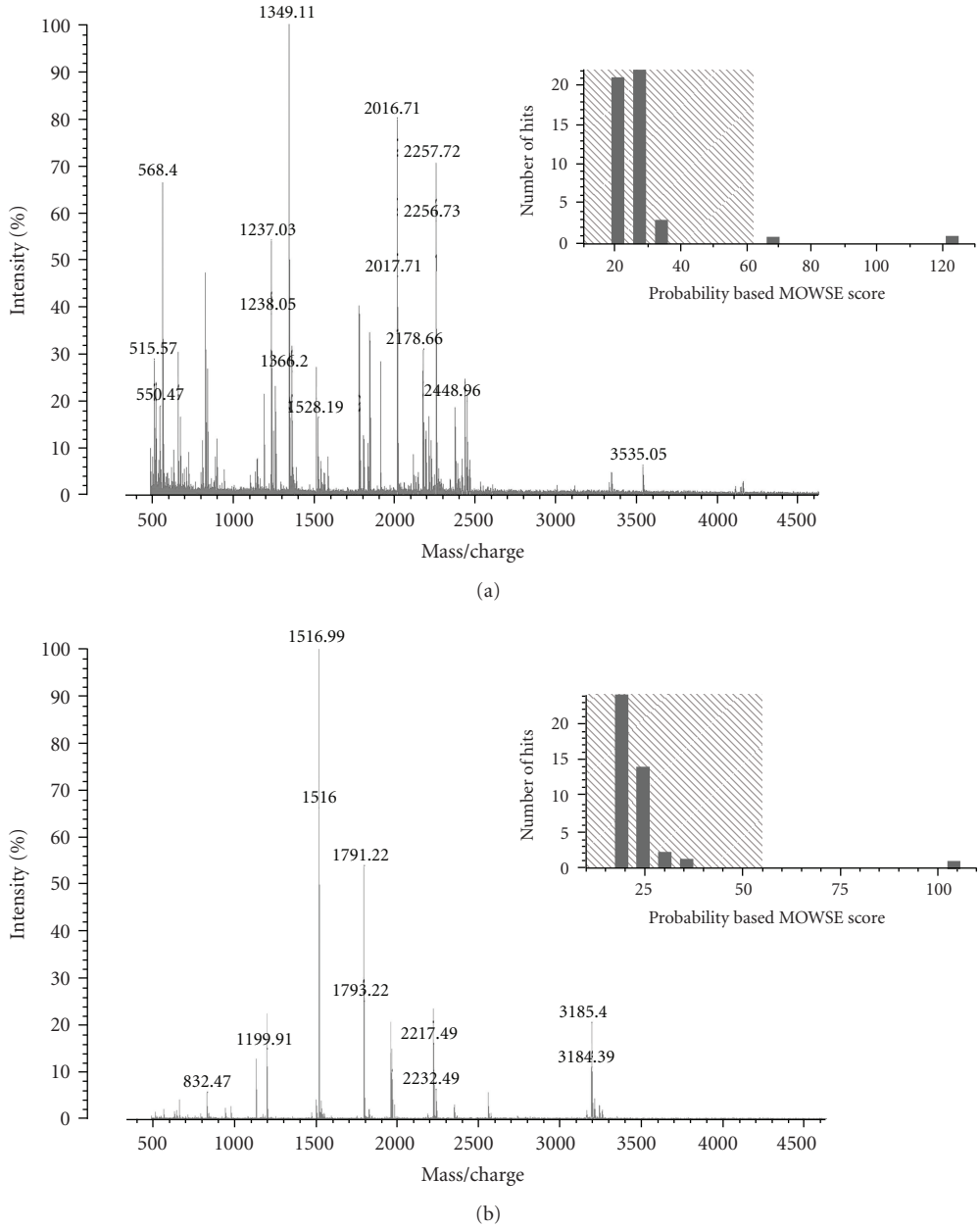

Figure 3: MALDI-TOF MS peptide mass fingerprints (PMFs) of (a) HSP-90, with inset showing probability-based MOWSE scores of 123 and 71 for the β and α isoforms, respectively, and (b) actin, with inset showing probability-based MOWSE scores of 103 for both the β and γ isoforms. Proteins were identified by their PMF utilizing MASCOT software against the NCBI and Swiss-Prot databases.

When α-SM actin, this time stained red in the absence of DAPI for enhanced visibility, is examined alone on these surfaces (Figures 6(b), 6(d), 6(f), and 6(h)) diminished expression of α-SM actin filaments is again observed on glass (Figure 6(b)) and $(PDADMA/PSS)_2$ (Figure 6(d)), and again, the filaments largely avoid the central regions of the cell. In contrast, the abundance of α-SM actin fibers observed on $(PFPVP/Nafion)_2$ (Figure 6(f)) fill the cytoplasm, extending from one end of the cell to the other, while staining of the cells on $(PAH/PAA\text{-}co\text{-}PAEDAPS)_2$ yield only a haze of unpolymerized actin (Figure 6(h)), with any filaments that might be present beyond the limits of detection.

3.5. Intracellular Localization of Vimentin. The cytoskeletal protein vimentin was also identified from excised spots (MOWSE: 156, sequence coverage: 56%), and while subsequent blotting experiments failed to show differential expression of this protein (data not shown), fluorescent immunostaining revealed striking differences in the cellular localization of vimentin. On glass (Figure 7(a)), vimentin expression is seen primarily in the cytoplasmic area surrounding the nucleus, with only minimal expression in the extended, stellate regions of the cell. The opposite trend is observed on $(PFPVP/Nafion)_2$ (Figure 7(b)), with staining throughout the cytoplasm that extends to the outermost

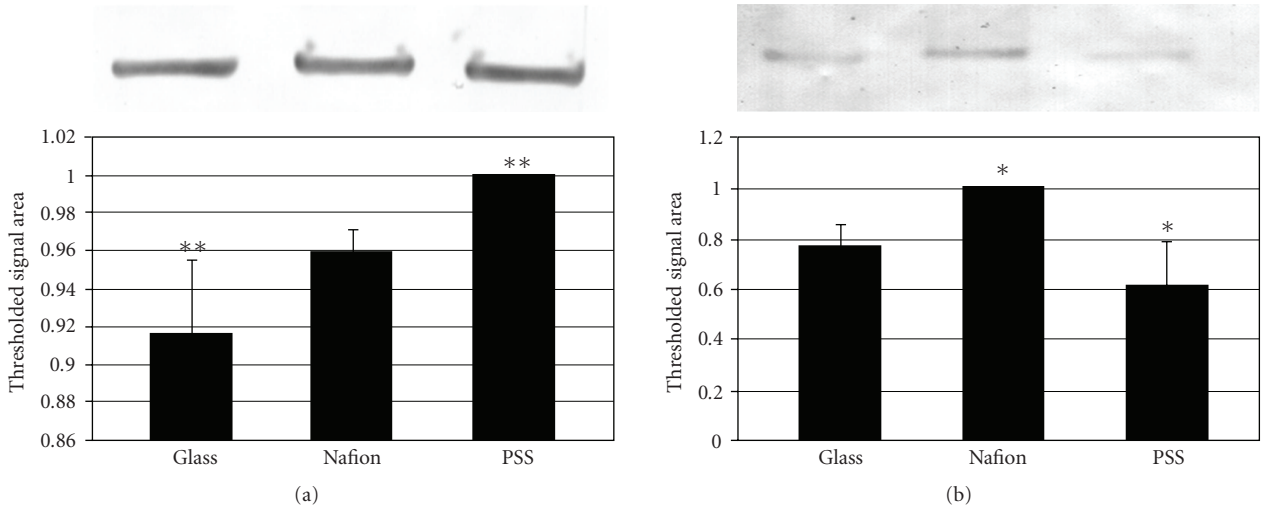

Figure 4: Western blot analysis of (a) HSP90 and (b) α-SM actin. Blots represent 5 μg of total protein from cell lysates, with each series of blots repeated three times. Histograms show the volume of bands expressed as a percentage of the maximum band in the presence of a uniform threshold applied to each series of blots. $(PDADMA/PSS)_2$ consistently generated the maximum threshold for HSP90 blots, and $(PFPVP/Nafion)_2$ consistently generated the maximum threshold when blots were probed specifically for α-SM actin (exclusive of other isoforms). Significant variation was seen in the expression of HSP90 when $(PDADMA/PSS)_2$ was compared to uncoated glass, and in the expression of α-SM actin when $(PFPVP/Nafion)_2$ was compared to $(PDADMA/PSS)_2$. Values are expressed as the mean ± S.E., with variations in the means compared by 1-way ANOVA. *CI = 90%, **CI = 95%.

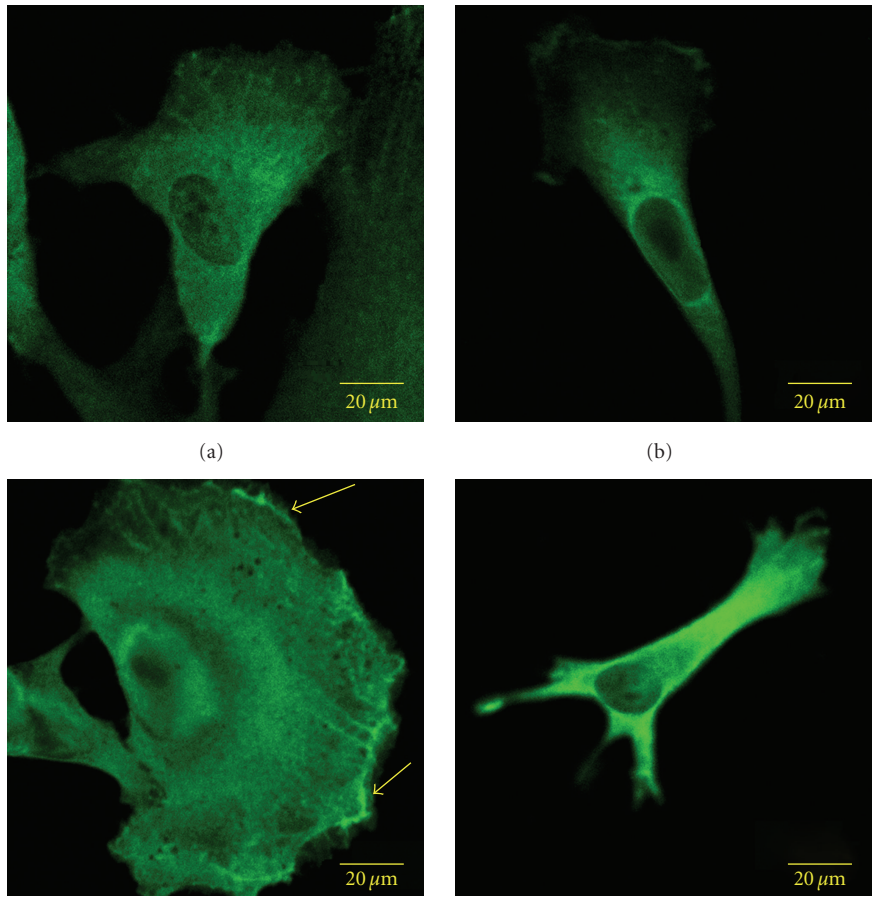

Figure 5: Fluorescent staining for HSP90 on (a) uncoated glass, (b) $(PFPVP/Nafion)_2$, (c) $(PDADMA/PSS)_2$, and (d) (PAH/PAA-*co*-PAEDAPS)$_2$. Positive signals were detected with the Alexa Fluor 488 secondary antibody, conjugated to a green fluorophore. Yellow arrows (c) designate areas of concentrated HSP90 expression at the leading edge of cells on the $(PDADMA/PSS)_2$ surface.

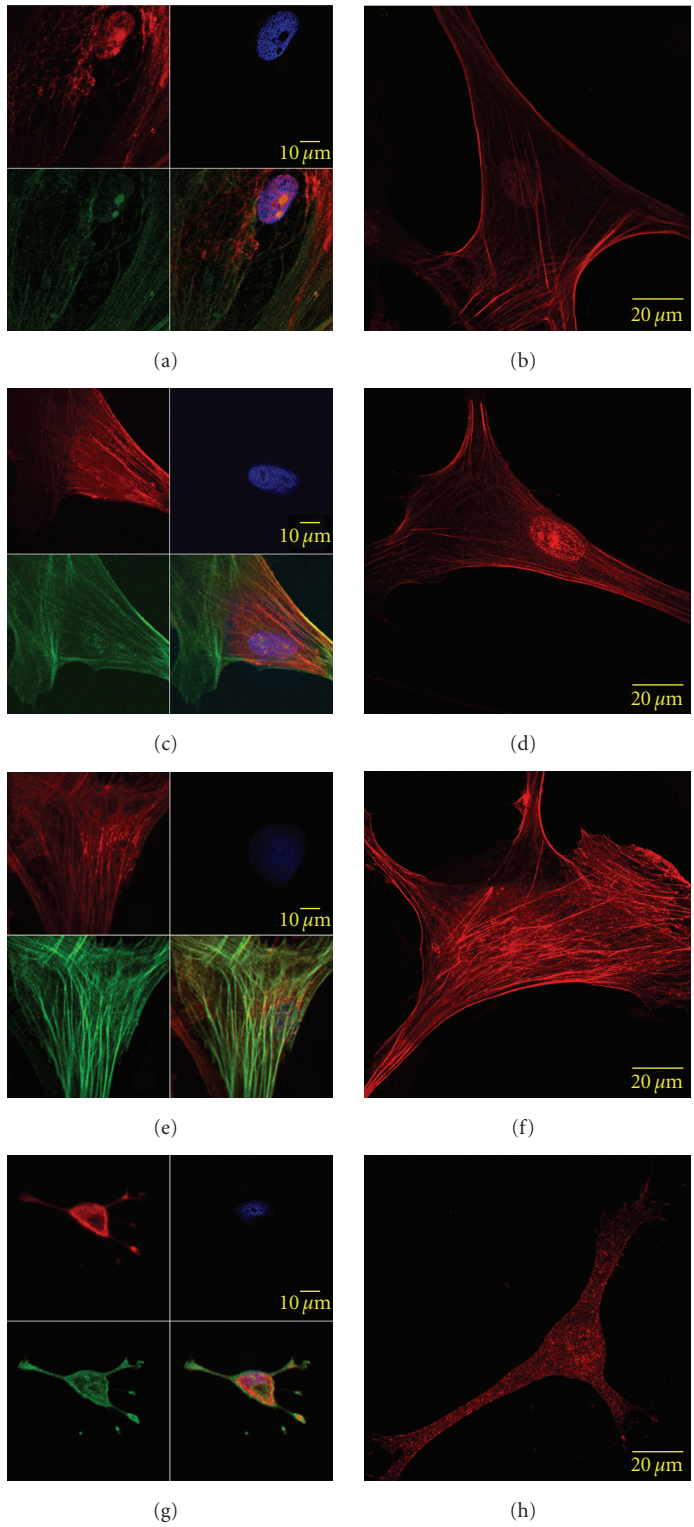

Figure 6: Fluorescent double staining for multiple actin isoforms (red) and α-SM actin (green) on (a) uncoated glass, (c) $(PDADMA/PSS)_2$, (e) $(PFPVP/Nafion)_2$, and (g) $(PAH/PAA\text{-}co\text{-}PAEDAPS)_2$. Positive signals were detected with Alexa Fluor 488 (green) and Alexa Fluor 546 (red) secondary antibodies. For double-stained images, nuclei are stained blue with DAPI. For enhanced clarity of the observed trends in α-SM actin patterns of expression, fluorescent staining exclusive for α-SM actin (red) in the absence of DAPI is shown on (b) uncoated glass, (d) $(PDADMA/PSS)_2$, (f) $(PFPVP/Nafion)_2$, and (h) $(PAH/PAA\text{-}co\text{-}PAEDAPS)_2$, utilizing the Alexa Fluor 546 secondary antibody.

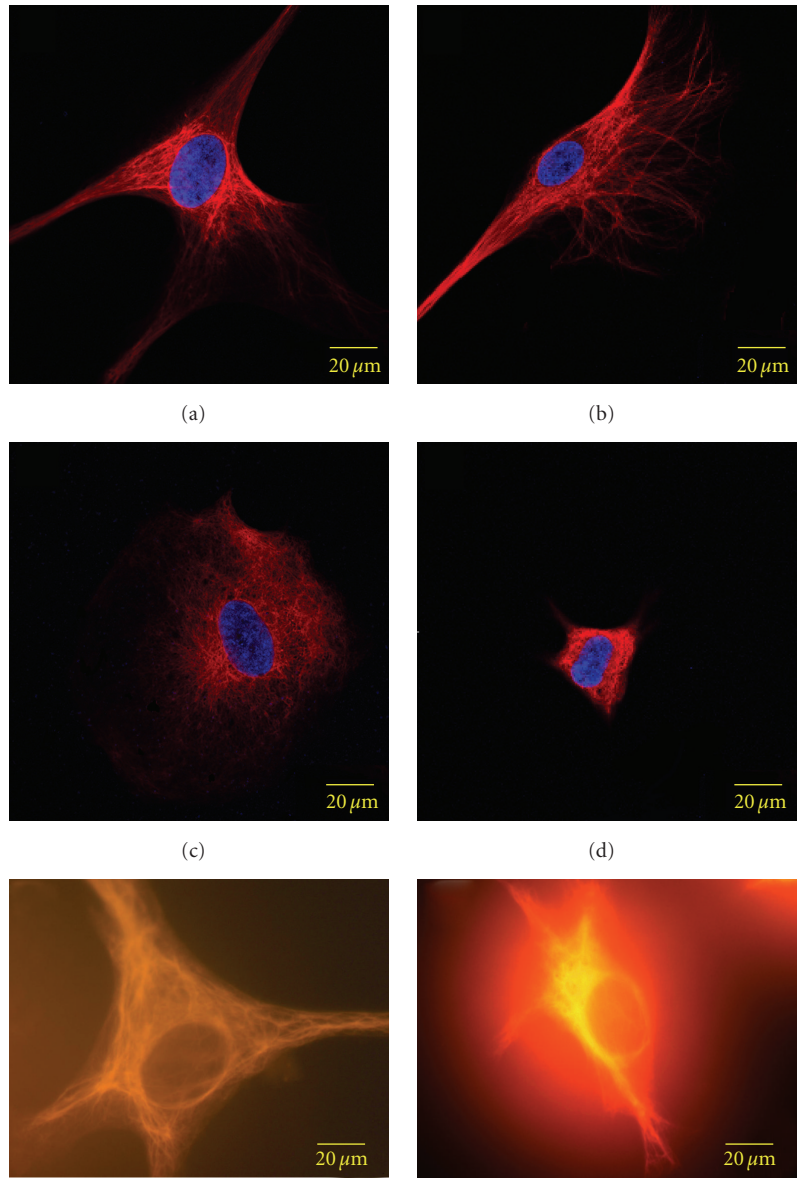

Figure 7: Fluorescent staining for vimentin on (a) uncoated glass, (b) $(PFPVP/Nafion)_2$, (c, e) $(PDADMA/PSS)_2$, and (d, f) (PAH/PAA-*co*-$PAEDAPS)_2$. The top four images (a)–(d) are confocal microscopy images in which positive signals are detected with the Alexa Fluor 546 secondary antibody conjugated to a red fluorophore, and cell nuclei are stained blue with DAPI. The lower images (e, f) are wide-field images at the same magnification for enhanced visualization of (e) the fine mesh of intermediate filaments on the $(PDADMA/PSS)_2$ surface and (f) formation of the condensed "nuclear cap" on the (PAH/PAA-*co*-$PAEDAPS)_2$ surface.

regions of the cell, and an alignment that might imply association with a contractile microfilament network. The $(PDADMA/PSS)_2$ cultures offer a third pattern of vimentin expression (Figure 7(c)), revealed by wide-field fluorescence (Figure 7(e)) as a fine meshwork of the sort most commonly ascribed to microtubule (MT) association. On (PAH/PAA-*co*-$PAEDAPS)_2$ surfaces, however, all evidence of vimentin organization has vanished, with no indications of any cytoskeletal structure whatsoever (Figure 7(d)). In many cell types the absence of MT filaments is associated with a localization of vimentin to a perinuclear "cap" [32]. The evidence for such an occurrence in the (PAH/PAA-*co*-$PAEDAPS)_2$ cultures is supported by wide-field images (Figure 7(f)) in which the signals for vimentin expression at the "nuclear cap" are so strong and condensed that they virtually overwhelm any other details in the image.

3.6. Cell Contraction on $(PFPVP/Nafion)_2$. As described previously, confluent hCASMC cultures on $(PFPVP/Nafion)_2$ adopt a "hill and valley" morphology (Figure 8(a)), with tightly packed areas of high cell density (the hills) being separated by sparser areas populated with a lower density

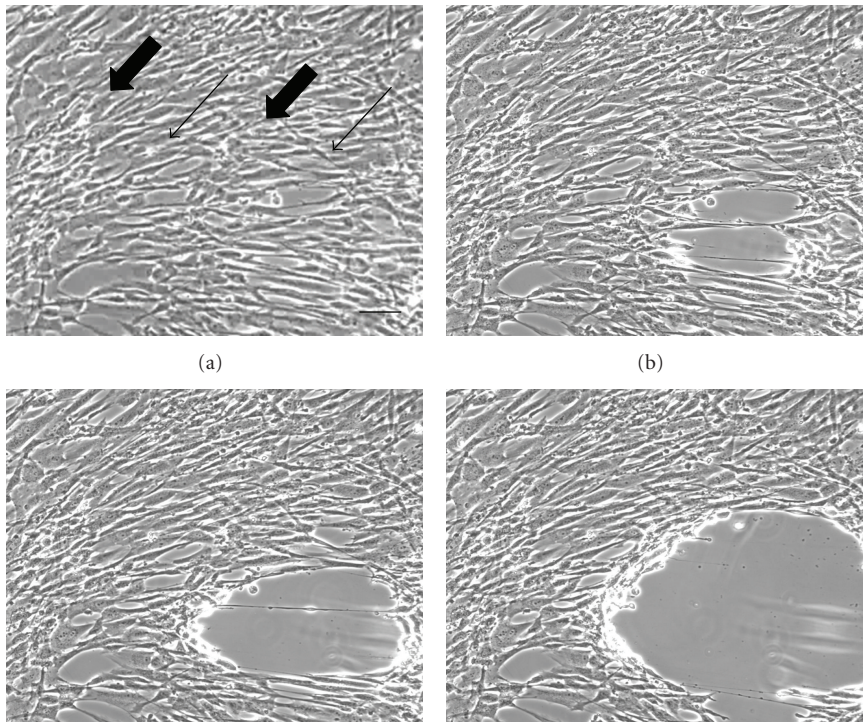

Figure 8: Contraction of hCASMC culture on a $(PFPVP/Nafion)_2$ surface. Images are shown at (a) 0 minutes, (b) 2.5 minutes, (c) 3.5 minutes, and (d) 5 minutes after the initiation of contraction using the A23187 ionophore. A contractile "hill and valley" morphology (a) is illustrated by the thick arrows ("hills") and the thin arrows ("valleys"). This response was not observed on glass or $(PDADMA/PSS)_2$ cultures exposed to the A23187 ionophore, nor was it seen in control $(PFPVP/Nafion)_2$ cultures exposed to SmBM/DMSO alone, which served as the vehicle for A23187 delivery (data not shown). $(PAH/PAA\text{-}co\text{-}PAEDAPS)_2$ cultures were not tested by these methods. Representative image stills are from an image stack of 100 images, all taken at 100x and processed using Metamorph Systems. Scale bar = 20 μm.

of elongated cells (the valleys) [5, 28]. When cultures of this type undergo contraction, induced here by the A23187 ionophore, the sparsely populated valleys are ravaged by the lateral pulling forces from the hills that surround them on either side. Over the course of approximately five minutes (Figures 8(a)–8(d)), the cells in these less populous regions are pulled taut by the neighboring cells in denser regions before they finally give way, as the forcible detachment of adhesion sites is common during contraction in culture systems [30]. Once contraction has ceased, multiple holes (Figure 8(d)) are found scattered throughout the valleys of the culture, while the dense hills have become denser still. This response was not observed on glass or $(PDADMA/PSS)_2$ cultures exposed to the A23187 ionophore, nor was it seen in control $(PFPVP/Nafion)_2$ cultures exposed to DMSO alone, which served as the vehicle for A23187 delivery. $(PAH/PAA\text{-}co\text{-}PAEDAPS)_2$ cultures were not tested by these methods.

4. Discussion

This study demonstrates that PEMU surfaces can be used to alter many characteristics of hCASMCs in culture, and that some of these alterations are consistent with changes linked to phenotypic modulation. Previous investigations utilizing a rat aortic smooth muscle cell line (A7r5) and a panel of PEMU coatings revealed dramatic effects on cell attachment and cell spreading based upon the hydrophobicity and surface charge of these growth surfaces, with hydrophobic films carrying a negative charge exhibiting the greatest degree of cytophilicity, while a novel, hydrophilic zwitterion displayed remarkable resistance to cell attachment [19, 20]. The three PEMU surfaces selected from these prior studies for further analysis here are referred to now for simplicity as "Nafion", "PSS", and "PAA-*co*-PAEDAPS", in each instance referencing the outermost layer contacting the ventral surface of the attaching cells. Each PEMU surface was prepared utilizing layer-by-layer deposition [9, 10] at a thickness of two layer pairs to minimize swelling in buffer solution, as the hydration and swelling of these films can play a significant role in nonadhesion [11, 33, 34]. Each of the topmost layers terminate with a sulfonate as their outermost functional group, lending each of these surfaces a negative charge, or in the case of the zwitterionic PAA-*co*-PAEDAPS, a net negative charge. The Nafion, PSS, and PAA-*co*-PAEDAPS surfaces vary in their hydrophobicity, with water contact angles of 100 ($\pm 5^\circ$), 30 ($\pm 3^\circ$), and 10 ($\pm 2^\circ$), respectively [19]. As each surface was coated onto glass, uncoated glass coverslips, which naturally carry a negative charge, were utilized for comparison.

Nafion and PSS were selected in part for the demonstrated biocompatibility. Nafion is resistant to damage by blood [35] and has demonstrated utility as a component in glucose biosensor systems for the management of diabetes mellitus [36, 37]. PSS is similarly biocompatible and has therapeutic utility as a potassium-binding resin for the treatment of elevated potassium levels commonly known as hyperkalemia [38]. PAA-*co*-PAEDAPS was designed to mimic biological surfaces [19], as the majority of membrane phospholipid headgroups posses a zwitterionic character, but when included in a copolymer formulation at even a modest concentration of 10%, PAA-*co*-PAEDAPS exhibits a near-total resistance to cell attachment.

The growth of human cells on these selected PEMU surfaces was diminished compared to glass in every instance, most significantly so in the case of PAA-*co*-PAEDAPS. While cellular behaviors on PEMU films are likely to be a function of multiple factors as opposed to a single parameter [15], reduced proliferation would be expected in the Nafion cultures if indeed characteristics of the less proliferative contractile phenotype were present. While there is no evidence for similar assumptions in the PSS cultures, it is also possible that the formation of cell aggregates on PSS led to an early onset of normal contact inhibition [28].

Aside from the morphological findings, the presence of different phenotypes in these cultures is further suggested by the observed fluctuations in protein expression. While variations in the expression of HSP90 and actin were not profound in their magnitude, it is rather the intracellular localization of these proteins that suggests alterations in the cellular machinery that may be indicative of alternate phenotypes. The highly localized areas of HSP90 found at the leading edge of cell membrane ruffles in hCASMCs cultured on PSS (Figure 5(c)) are intriguing given that the HSP90α isoform is secreted extracellularly in an invasive human breast cancer cell line (MDA-MB-231), where it likely contributes to the activation of matrix metalloproteinase-2 (gelatinase A, MMP-2), a potent proteolytic enzyme responsible for the digestion of many extracellular matrix (ECM) components by invasive cells [39]. Many of the paradigms of tumor cell invasion, such as increased migration through digested ECM, are similar to the processes at play during the early stages of restenosis, as SMCs migrate from the arterial media towards the lumen, and while increased MMP expression is observed after coronary angioplasty in the presence or absence of stent placement [40], the activation of MMP-2 is even more pronounced in the wake of stent implantation [41]. Thus, hCASMCs cultured on PSS imply an invasive potential that is absent on the remainder of the surfaces, suggesting that gelatinase activation might provide one mechanism by which the HSPs contribute to hCASMC invasion through the ECM that would otherwise confine them.

Invasion by hCASMCs is representative of the synthetic phenotype, however, and the primary physiologic function of mature, contractile hCASMCs is the maintenance of blood flow and vascular tone [4]. The transition to a synthetic phenotype is associated with a loss of contractility, and alterations in both the expression and localization of cytoskeletal and contractile proteins, such as actin, accompany this modulation [3]; in rat aortic (A7r5) SMCs, exposure to tumor-promoting phorbol esters has been shown to induce a dedifferentiated state [42] that is associated with a 70% decrease in α-SM actin stress fibers [43]. Of the surfaces examined here, it is the well-developed network of α-SM actin microfilaments on Nafion that appear the most consistent with and the most poised for potential contraction events. Also of note is the curious amount of nuclear actin staining observed on PSS, and while this is potentially an artifact, it was not observed on the other surfaces that were fixed and stained using identical protocols. Actin is typically considered a cytoplasmic protein, but actin transport into the nucleus might nevertheless be mediated by binding partners with nuclear location signals, such as cofilin, or simple diffusion might also accomplish this task, as nuclear pores are sufficiently wide to allow for the passage of actin monomers [44].

Apart from actin, the expression of many cytoskeletal proteins can serve as useful benchmarks in describing the differentiated state of SMCs [1], as phenotypic modulation is associated with numerous changes in the intracellular localization of cytoskeletal proteins as contractile function is gained or lost [3]. Another key cytoskeletal protein is vimentin, a class III intermediate filament (IF) protein that is primarily expressed in mesenchyme-derived cells, a group that includes both endothelial and vascular SMCs [45]. Vimentin frequently coaligns with microtubule networks, but has also been observed to form a meshwork that ensheaths cellular stress fibers [3], suggesting that vimentin may also participate in the regulation of vascular tone [46], or in the stabilization of microtubules, providing lateral support and stability to microtubules that might otherwise buckle during cell contraction [47]. There are reports that the expression of vimentin varies in rabbit SMCs grown on collagen IV to induce contractile phenotypes [3], and conflicting reports that vimentin is amongst the cytoskeletal proteins that remain constant in porcine SMCs induced into phenotypic modulation by serum withdrawal [8]. The levels of vimentin expression were found to remain constant under the conditions of this study, but there was a striking variety in intracellular localization that occurred independent of any changes in magnitude. The filament-like fibers seen on Nafion that extend the length of the cell contrast starkly with the fine meshwork of strands observed on PSS (Figure 7). This latter pattern of expression may be indicative of a well-developed microtubule network and an increase in the synthesis of proteins requiring vesicular transport, or there may be a decrease in the amount of filamentous α-SM actin available for vimentin association (Figures 6(c) and 6(d)), or perhaps a combination of both factors is at play, as neither of these possibilities is at odds with the other. The striking formation of the "nuclear cap" in the PAA-*co*-PAEDAPS cells implies not only aberrant signaling processes in these cells, as a lack of vimentin impairs the transduction of chemical and mechanical stimuli from the vessel wall [46], but also a disturbed spatial organization of focal contact proteins and a disruption of actin microfilament organization [48].

To ascertain the presence of a functional contractile apparatus in these cells, particularly in Nafion cultures that exhibited a "hill and valley" morphology [5, 28] combined with cytoskeletal features consistent with contraction, the antibiotic A23187 (calcimycin, MW 523.6 g/mol) was utilized as an ionophore to facilitate the transmembrane transport of calcium ions [49]. A23187 selectively binds calcium ions with a 1 : 1 stoichiometry [50, 51], exchanging two protons for a divalent metal ion to form a neutral species that shields the charge of the ion during transport through the hydrophobic interior of the lipid bilayer, increasing intracellular stores of calcium and inducing contraction [52]. When cultures grown to confluence on Nafion surfaces where exposed to this ionophore at a concentration of 1 μM, contraction was observed in these systems over the course of several minutes.

In conclusion, evidence is presented here that layer-by-layer assembled PEMU films can indeed elicit a variety of in vitro cellular responses from cultured hCASMCs in terms of growth, morphology, protein expression, and the organization, formation, or suppression of cytoskeletal structures. Nafion-coated surfaces prompt the formation of a well-developed network of α-SM actin microfilaments that spans the cytoplasm and can be induced to contract. On PSS surfaces, hCASMCs are most similar to those cultured on uncoated glass, where perinuclear evacuation of α-SM actin microfilaments implies an increased presence of synthetic organelles, but a unique invasive potential is also suggested by HSP90 localization to membrane ruffles at the leading edge. On PAA-*co*-PAEDAPS, hCASMCs exhibit a total absence of visible actin microfilaments and the formation of a vimentin nuclear cap, implying the suppression of key cytoskeletal components. These findings support an emerging utility for PEMU surfaces, with the potential to dictate cellular responses upon their introduction into specific biological milieus, given that one of the primary strengths of a multilayer coating strategy for implantable devices would be their influence upon cells most proximal to the device, exerting nonsystemic effects in the most localized fashion possible. Furthermore, control of the PEMU deposition parameters affords the opportunity to fine-tune these surfaces so as to direct or deter the growth and attachment of selected cell types, or in the case of hCASMCs, potentially influence the resultant phenotype of attaching cells.

Acknowledgments

This work was supported in part by a Predoctoral Fellowship (0415173B) from the American Heart Association Florida/Puerto Rico Affiliate (to R. G. Newcomer), Grants from the Florida State University (FSU) (to Q.-X. Sang and J. B. Schlenoff) and the National Institutes of Health 5R01EB006158 (to J. B. Schlenoff and T. C. S. Keller). The authors thank Dr. D. Terry of the FSU College of Medicine for her expert assistance with 2DE and MALDI-TOF-MS, and K. Riddle of the FSU Biological Science Imaging Resource for her technical assistance with all aspects of microscopy.

References

[1] S. M. Schwartz, G. R. Campbell, and J. H. Campbell, "Replication of smooth muscle cells in vascular disease," *Circulation Research*, vol. 58, no. 4, pp. 427–444, 1986.

[2] M. G. Frid, E. P. Moiseeva, and K. R. Stenmark, "Multiple phenotypically distinct smooth muscle cell populations exist in the adult and developing bovine pulmonary arterial media in vivo," *Circulation Research*, vol. 75, no. 4, pp. 669–681, 1994.

[3] N. F. Worth, B. E. Rolfe, J. Song, and G. R. Campbell, "Vascular smooth muscle cell phenotypic modulation in culture is associated with reorganisation of contractile and cytoskeletal proteins," *Cell Motility and the Cytoskeleton*, vol. 49, no. 3, pp. 130–145, 2001.

[4] M. Sata, A. Saiura, A. Kunisato et al., "Hematopoietic stem cells differentiate into vascular cells that participate in the pathogenesis of atherosclerosis," *Nature Medicine*, vol. 8, no. 4, pp. 403–409, 2002.

[5] D. Simper, P. G. Stalboerger, C. J. Panetta, S. Wang, and N. M. Caplice, "Smooth muscle progenitor cells in human blood," *Circulation*, vol. 106, no. 10, pp. 1199–1204, 2002.

[6] H. Hao, G. Gabbiani, and M.-L. Bochaton-Piallat, "Arterial smooth muscle cell heterogeneity: implications for atherosclerosis and restenosis development," *Arteriosclerosis, Thrombosis, and Vascular Biology*, vol. 23, no. 9, pp. 1510–1520, 2003.

[7] G. K. Owens, M. S. Kumar, and B. R. Wamhoff, "Molecular regulation of vascular smooth muscle cell differentiation in development and disease," *Physiological Reviews*, vol. 84, no. 3, pp. 767–801, 2004.

[8] C. Boccardi, A. Cecchettini, A. Caselli et al., "A proteomic approach to the investigation of early events involved in vascular smooth muscle cell activation," *Cell and Tissue Research*, vol. 328, no. 1, pp. 185–195, 2007.

[9] G. Decher, "Fuzzy nanoassemblies: toward layered polymeric multicomposites," *Science*, vol. 277, no. 5330, pp. 1232–1237, 1997.

[10] G. Decher and J. B. Schlenoff, Eds., *Multilayer Thin Films—Sequential Assembly of Nanocomposite Materials*, Wiley-VCH, Weinheim, Germany, 2003.

[11] S. Y. Yang, J. D. Mendelsohn, and M. F. Rubner, "New class of ultrathin, highly cell-adhesion-resistant polyelectrolyte multilayers with micropatterning capabilities," *Biomacromolecules*, vol. 4, no. 4, pp. 987–994, 2003.

[12] S. Kidambi, I. Lee, and C. Chan, "Controlling primary hepatocyte adhesion and spreading on protein-free polyelectrolyte multilayer films," *Journal of the American Chemical Society*, vol. 126, no. 50, pp. 16286–16287, 2004.

[13] S. P. Forry, D. R. Reyes, M. Gaitan, and L. E. Locascio, "Facilitating the culture of mammalian nerve cells with polyelectrolyte multilayers," *Langmuir*, vol. 22, no. 13, pp. 5770–5775, 2006.

[14] C. Boura, P. Menu, E. Payan et al., "Endothelial cells grown on thin polyelectrolyte mutlilayered films: an evaluation of a new versatile surface modification," *Biomaterials*, vol. 24, no. 20, pp. 3521–3530, 2003.

[15] C. Boura, S. Muller, D. Vautier et al., "Endothelial cell—interactions with polyelectrolyte multilayer films," *Biomaterials*, vol. 26, no. 22, pp. 4568–4575, 2005.

[16] N. Berthelemy, H. Kerdjoudj, C. Gaucher et al., "Polyelectrolyte films boost progenitor cell differentiation into endothelium-like monolayers," *Advanced Materials*, vol. 20, no. 14, pp. 2674–2678, 2008.

[17] H. Kerdjoudj, N. Berthelemy, S. Rinckenbach et al., "Small vessel replacement by human umbilical arteries with polyelectrolyte film-treated arteries. In vivo behavior," *Journal of the American College of Cardiology*, vol. 52, no. 19, pp. 1589–1597, 2008.

[18] N. Berthelemy, H. Kerdjoudj, P. Schaaf et al., "O2 level controls hematopoietic circulating progenitor cells differentiation into endothelial or smooth muscle cells," *PloS one*, vol. 4, no. 5, article e5514, 2009.

[19] D. S. Salloum, S. G. Olenych, T. C. S. Keller, and J. B. Schlenoff, "Vascular smooth muscle cells on polyelectrolyte multilayers: hydrophobicity-directed adhesion and growth," *Biomacromolecules*, vol. 6, no. 1, pp. 161–167, 2005.

[20] S. G. Olenych, M. D. Moussallem, D. S. Salloum, J. B. Schlenoff, and T. C. S. Keller, "Fibronectin and cell attachment to cell and protein resistant polyelectrolyte surfaces," *Biomacromolecules*, vol. 6, no. 6, pp. 3252–3258, 2005.

[21] M. D. Moussallem, S. G. Olenych, S. L. Scott, T. C. S. Keller III, and J. B. Schlenoff, "Smooth muscle cell phenotype modulation and contraction on native and cross-linked polyelectrolyte multilayers," *Biomacromolecules*, vol. 10, no. 11, pp. 3062–3068, 2009.

[22] S. J. Assinder, J.-A. L. Stanton, and P. D. Prasad, "Transgelin: an actin-binding protein and tumour suppressor," *International Journal of Biochemistry and Cell Biology*, vol. 41, no. 3, pp. 482–486, 2009.

[23] A. J. Engler, C. Carag-Krieger, C. P. Johnson et al., "Embryonic cardiomyocytes beat best on a matrix with heart-like elasticity: scar-like rigidity inhibits beating," *Journal of Cell Science*, vol. 121, no. 22, pp. 3794–3802, 2008.

[24] C. L. McCormick and L. C. Salazar, "Water soluble copolymers: 46. Hydrophilic sulphobetaine copolymers of acrylamide and 3-(2-acrylamido-2-methylpropanedimethylammonio)-1-propanesulphonate," *Polymer*, vol. 33, no. 21, pp. 4617–4624, 1992.

[25] R. M. Ji Sr., H. H. Rmaile, and J. B. Schlenoff, "Hydrophobic and ultrahydrophobic multilayer thin films from perfluorinated polyelectrolytes," *Angewandte Chemie—International Edition*, vol. 44, no. 5, pp. 782–785, 2005.

[26] S. Diziain, J. Dejeu, L. Buisson, D. Charraut, F. Membrey, and A. Foissy, "Investigations in the initial build-up stages of polyelectrolyte multilayers by laser reflectometry and atomic force microscopy," *Thin Solid Films*, vol. 516, no. 1, pp. 1–7, 2007.

[27] S. Mehrotra, S. C. Hunley, K. M. Pawelec et al., "Cell adhesive behavior on thin polyelectrolyte multilayers: cells attempt to achieve homeostasis of its adhesion energy," *Langmuir*, vol. 26, no. 15, pp. 12794–12802, 2010.

[28] P. L. Faries, D. I. Rohan, H. Takahara et al., "Human vascular smooth muscle cells of diabetic origin exhibit increased proliferation, adhesion, and migration," *Journal of Vascular Surgery*, vol. 33, no. 3, pp. 601–607, 2001.

[29] D. Picard, "Hsp90 invades the outside," *Nature Cell Biology*, vol. 6, no. 6, pp. 479–480, 2004.

[30] M. E. Fultz, C. Li, W. Geng, and G. L. Wright, "Remodeling of the actin cytoskeleton in the contracting A7r5 smooth muscle cell," *Journal of Muscle Research and Cell Motility*, vol. 21, no. 8, pp. 775–787, 2000.

[31] S. Koyasu, E. Nishida, T. Kadowaki et al., "Two mammalian heat shock proteins, HSP90 and HSP100, are actin-binding proteins," *Proceedings of the National Academy of Sciences of the United States of America*, vol. 83, no. 21, pp. 8054–8058, 1986.

[32] F. K. Gyoeva and V. I. Gelfand, "Coalignment of vimentin intermediate filaments with microtubules depends on kinesin," *Nature*, vol. 353, no. 6343, pp. 445–448, 1991.

[33] C. Picart, J. Mutterer, L. Richert et al., "Molecular basis for the explanation of the exponential growth of polyelectrolyte multilayers," *Proceedings of the National Academy of Sciences of the United States of America*, vol. 99, no. 20, pp. 12531–12535, 2002.

[34] L. Richert, P. Lavalle, E. Payan et al., "Layer by layer buildup of polysaccharide films: physical chemistry and cellular adhesion aspects," *Langmuir*, vol. 20, no. 2, pp. 448–458, 2004.

[35] C. Heitner-Wirguin, "Recent advances in perfluorinated ionomer membranes: structure, properties and applications," *Journal of Membrane Science*, vol. 120, no. 1, pp. 1–33, 1996.

[36] W. K. Ward, L. B. Jansen, E. Anderson, G. Reach, J.-C. Klein, and G. S. Wilson, "A new amperometric glucose microsensor: in vitro and short-term in vivo evaluation," *Biosensors and Bioelectronics*, vol. 17, no. 3, pp. 181–189, 2002.

[37] X. Kang, Z. Mai, X. Zou, P. Cai, and J. Mo, "A sensitive nonenzymatic glucose sensor in alkaline media with a copper nanocluster/multiwall carbon nanotube-modified glassy carbon electrode," *Analytical Biochemistry*, vol. 363, no. 1, pp. 143–150, 2007.

[38] S. Inaba, K. Nibu, H. Takano et al., "Potassium-adsorption filter for RBC transfusion: a phase III clinical trial," *Transfusion*, vol. 40, no. 12, pp. 1469–1474, 2000.

[39] B. K. Eustace, T. Sakurai, J. K. Stewart et al., "Functional proteomic screens reveal an essential extracellular role for hsp90α in cancer cell invasiveness," *Nature Cell Biology*, vol. 6, no. 6, pp. 507–514, 2004.

[40] M. J. Sierevogel, G. Pasterkamp, D. P. V. de Kleijn, and B. H. Strauss, "Matrix metalloproteinases: a therapeutic target in cardiovascular disease," *Current Pharmaceutical Design*, vol. 9, no. 13, pp. 1033–1040, 2003.

[41] L. J. Feldman, M. Mazighi, A. Scheuble et al., "Differential expression of matrix metalloproteinases after stent implantation and balloon angioplasty in the hypercholesterolemic rabbit," *Circulation*, vol. 103, no. 25, pp. 3117–3122, 2001.

[42] G. Burgstaller and M. Gimona, "Podosome-mediated matrix resorption and cell motility in vascular smooth muscle cells," *American Journal of Physiology—Heart and Circulatory Physiology*, vol. 288, no. 6, pp. H3001–H3005, 2005.

[43] D. Brown, A. Dykes, J. Black, S. Thatcher, M. E. Fultz, and G. L. Wright, "Differential actin isoform reorganization in the contracting A7r5 cell," *Canadian Journal of Physiology and Pharmacology*, vol. 84, no. 8-9, pp. 867–875, 2006.

[44] B. M. Jockusch, C.-A. Schoenenberger, J. Stetefeld, and U. Aebi, "Tracking down the different forms of nuclear actin," *Trends in Cell Biology*, vol. 16, no. 8, pp. 391–396, 2006.

[45] E. Fuchs and K. Weber, "Intermediate filaments: structure, dynamics, function, and disease," *Annual Review of Biochemistry*, vol. 63, pp. 345–382, 1994.

[46] F. Terzi, D. Henrion, E. Colucci-Guyon et al., "Reduction of renal mass is lethal in mice lacking vimentin: role of endothelin-nitric oxide imbalance," *Journal of Clinical Investigation*, vol. 100, no. 6, pp. 1520–1528, 1997.

[47] N. Wang and D. Stamenovic, "Mechanics of vimentin intermediate filaments," *Journal of Muscle Research and Cell Motility*, vol. 23, no. 5-6, pp. 535–540, 2002.

[48] B. Eckes, D. Dogic, E. Colucci-Guyon et al., "Impaired mechanical stability, migration and contractile capacity in vimentin deficient fibroblasts," *Journal of Cell Science*, vol. 111, no. 13, pp. 1897–1907, 1998.

[49] J. J. Murray, P. W. Reed, and F. S. Fay, "Contraction of isolated smooth muscle cells by ionophore A23187," *Proceedings of the National Academy of Sciences of the United States of America*, vol. 72, no. 11, pp. 4459–4463, 1975.

[50] M. A. Kolber and D. H. Haynes, "Fluorescence study of the divalent cation-transport mechanism of ionophore A23187 in phospholipid membranes," *Biophysical Journal*, vol. 36, no. 2, pp. 369–391, 1981.

[51] C. J. Chapman, A. K. Puri, R. W. Taylor, and D. R. Pfeiffer, "General features in the stoichiometry and stability of ionophore A23187-cation complexes in homogeneous solution," *Archives of Biochemistry and Biophysics*, vol. 281, no. 1, pp. 44–57, 1990.

[52] C. M. Deber and D. R. Pfeiffer, "Ionophore A23187. Solution conformations of the calcium complex and free acid deduced from proton and carbon-13 nuclear magnetic resonance studies," *Biochemistry*, vol. 15, no. 1, pp. 132–141, 1976.